

Supporting Information

Controlled Morphology Synthesis of Nanostructured $\beta\text{-AlF}_{3-x}(\text{OH})_x$ with Tunable Specific Surface Area

Valentine Camus-Génot, Amandine Guiet, Jérôme Lhoste, Franck Fayon, Monique Body,
Stéphanie Kodjikian, Romain Moury, Marc Leblanc, Jean Louis Bobet,
Christophe Legein,* Vincent Maisonneuve*

Table of Contents

Allotropic structures of AlF ₃	2
Design of Experiments (DoE) method	2
Rietveld refinements	4
Dielectric properties and boiling point of the different solvents	6
TEM image	6
Solid State NMR	7
¹⁹ F decoupling	7
Bibliographic data on ²⁷ Al δ_{iso} values of aluminum hydroxyfluorides and aluminum fluoride hydrate.....	7
²⁷ Al isotropic chemical shift ranges and quadrupolar coupling constants of the various AlF _{6-y} (OH) _y species and ¹⁹ F isotropic chemical shift ranges of the various FAl ₂ F _{10-z} (OH) _z species calculated using the DFT-GIPAW method for 2x1x1 supercell structural models	8
²⁷ Al MAS (33 kHz) NMR spectra of $\beta\text{-AlF}_{3-x}(\text{OH})_x$ samples	10
Structural data of $\beta\text{-AlF}_3$	11
¹⁹ F MAS experimental and reconstructed spectra of $\beta\text{-AlF}_{3-x}(\text{OH})_x$ samples	12
References	13

Allotropic structures of AlF₃

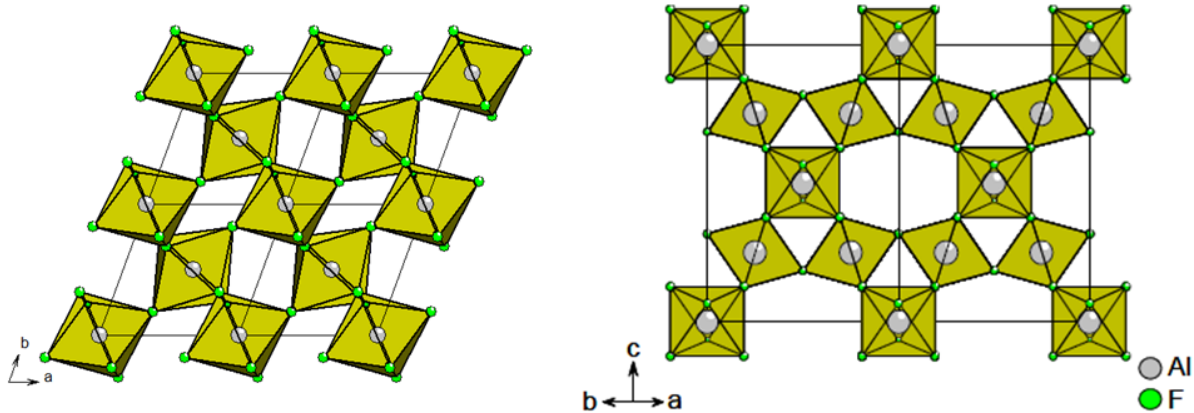


Figure S1. (left) [001] projection of the crystal structure of $\alpha\text{-AlF}_3$ which adopts a rhombohedral structure (VF₃ structure type) and (right) [110] projection of the crystal structure of $\eta\text{-AlF}_3$ which adopts a pyrochlore type structure.

Design of Experiments (DoE) method

The statistical DoE method is a powerful tool which focuses on how to plan and conduct experiments in order to extract the maximum amount of relevant information from the collected data with a minimum number of well-chosen experimental runs.¹ The basic idea is to vary all relevant parameters (referred to as factors) simultaneously over a set of planned experiments and then to connect the results by means of a mathematical model. The model is then used for interpretation, prediction and optimization. When only the main factor effects are of interest (this study), a screening DoE is implemented such as Plackett-Burman² or fractional factorial designs.¹ A screening DoE is very efficient to assess the impact of a large number of factors on the system properties characterized by a physical or chemical value referred to as a response. The response values are modelled with a first-order polynomial model represented by the following equation:

$$\hat{Y} = \beta_0 + \sum_{i=1}^k \beta_i X_i$$

where k denotes the number of factors, \hat{Y} is the predicted response, β_0 is the intercept constant, β_i are the linear coefficients and X_i are the coded variables. In this work, eight synthesis factors were investigated and each factor was considered at two levels (**Table S1**). Factors X1, X2, X3, X5, X6 are quantitative factors whose values can vary continuously between low and high levels, whereas factors X4, X7, X8 are qualitative ones, which can take only low or high settings. One of the interesting features of the DoE method is that quantitative and qualitative factors can be simultaneously investigated in the same design. The specific DoE software Modde 8.0 (Umetrics, Umea, Sweden) was used to build the design and perform mathematical and statistical analysis of the collected data. The model coefficients were assessed using multiple linear regressions. The coefficient of determination R^2 was evaluated as an indication of how well the model fits the response values and how much the variability in the response can be described by the model.

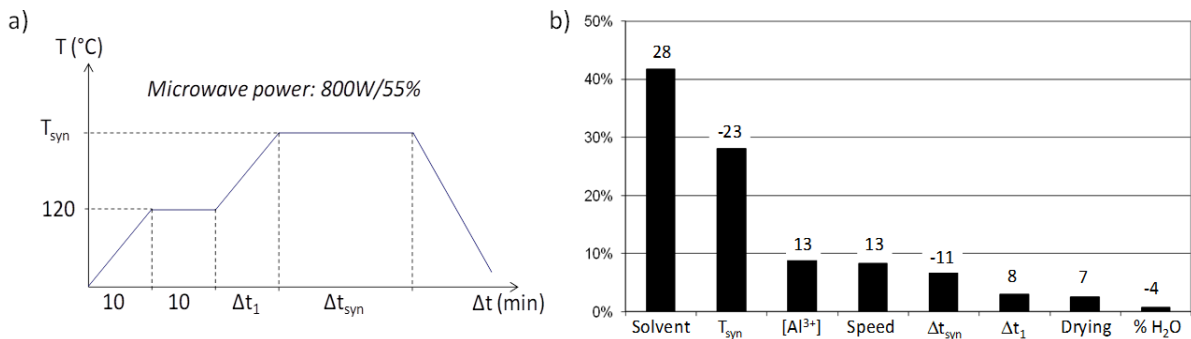


Figure S2. a) Temperature profile of the microwave assisted solvothermal reaction. b) Pareto chart of normalized squared pure effects of eight synthesis parameters on the S_{BET} response. Each pure effect value is indicated above the corresponding bar.

Table S1. Coded and actual levels for the 8 investigated factors: Heating rate (Δt_1 , min); Duration of the plateau (Δt_{syn} , min); Temperature of the plateau (T_{syn} , °C); Stirring speed; $[Al^{3+}]$ (mol.L⁻¹); Water proportion in the solvent (%); Solvent (Isopropanol ('PrOH) or Ethanol (EtOH)); Drying method.

Coded variable	Factor	Coded and actual levels	
		-1 (low)	+1 (high)
X ₁	Δt_1	10	15
X ₂	Δt_{syn}	30	60
X ₃	T _{syn}	130	150
X ₄	Stirring speed	low	medium
X ₅	$[Al^{3+}]$	0.5	0.9
X ₆	Water proportion	0	10
X ₇	Solvent	'PrOH	EtOH
X ₈	Drying method	classic	MW

For the drying process (factor X₈ in DoE, see **Table S1**), two drying methods were tested: the classical method consists of a simple filtering at room temperature whereas microwave (MW) drying involves a fast solvent evaporation by MW heating at 100°C during 15 minutes under primary vacuum. The resulting powders were washed with ethanol and acetone, dried at room temperature, sieved (125 µm) and finally outgassed at 150°C during 8 h under secondary vacuum.

Rietveld refinements

Table S2. Crystal data, data collection and structure refinement details. Crystal system: orthorhombic, space group: *Cmcm*. Radiation type: CuK α , 2 θ range (°): 10-100.

Sample	S-25	S-60	S-185	S-300	S-345
a (Å)	6.881(1)	6.888(1)	6.888(9)	6.881(20)	6.916(30)
b (Å)	11.872(1)	11.878(2)	11.926(2)	11.913(40)	11.878(50)
c (Å)	7.069(1)	7.075(1)	7.078(1)	7.023(2)	7.018(1)
V (Å ³)	577.4(1)	578.8(1)	582(2)	576(3)	577(3)
No of reflections	472	508	610	644	453
No of parameters	39	39	46	37	33
R _p /R _{wp}	0.181/0.128	0.150/0.118	0.109/0.095	0.193/0.133	0.204/0.146
R _B /R _f	0.042/0.081	0.034/0.060	0.026/0.028	0.038/0.055	0.020/0.049
χ^2	2.66	3.18	4.25	1.85	1.55
G1	1.00	1.00	0.92	0.69	0.52
<L> (Å)	25.5(2)	19.4(1)	11.4(1)	9.5(1)	6.6(1)

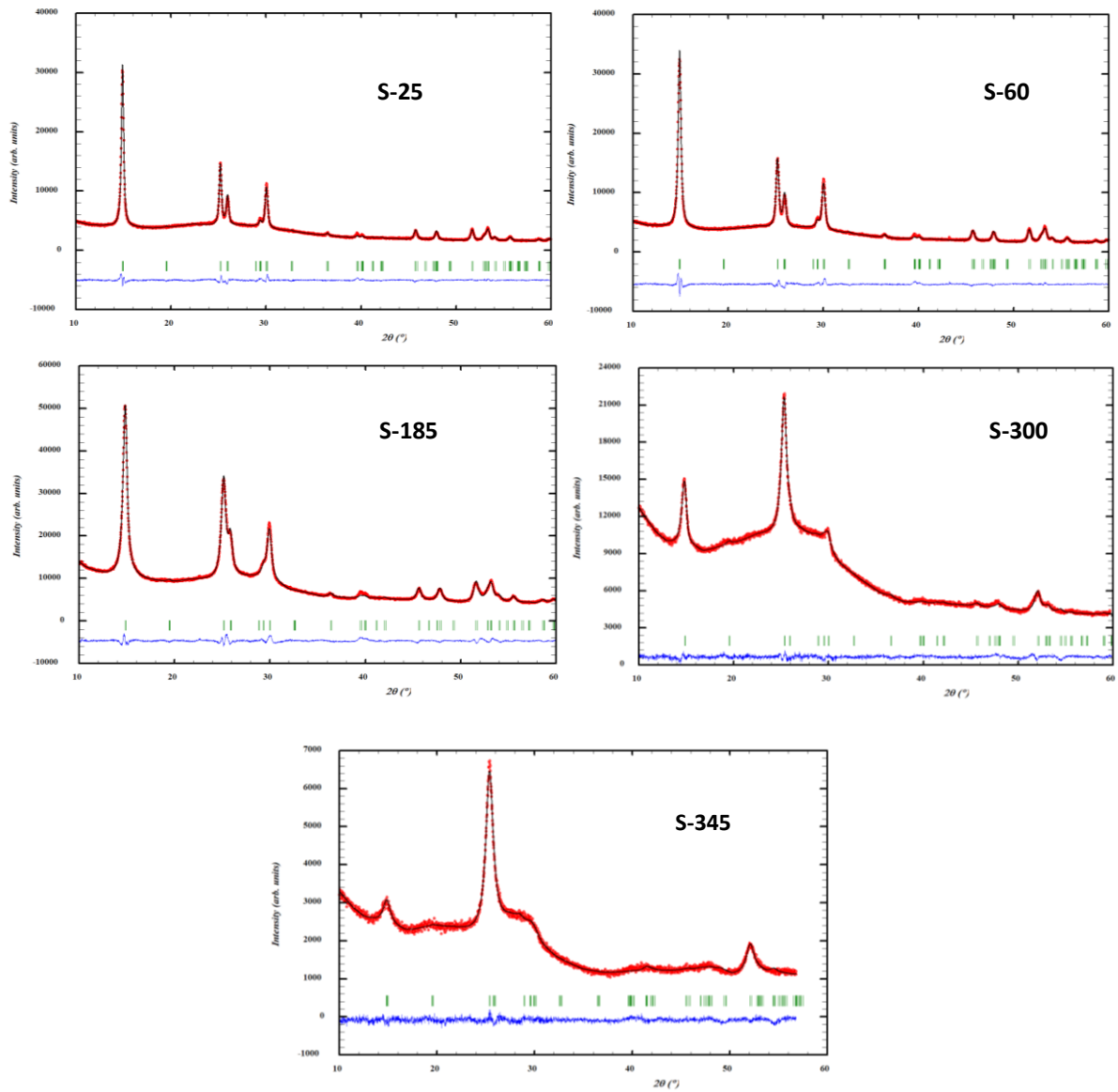


Figure S3. Rietveld refinements (SG: *Cmcm*) of the PXRD patterns of all the samples. Experimental (in black) and calculated (in red) patterns; Bragg positions (green vertical bars); difference between experimental and calculated patterns (in blue).

Dielectric properties and boiling point of the different solvents

Table S3. Dielectric properties (dielectric constant (ϵ'), dielectric loss (ϵ''), dissipation factor ($\tan \delta = \epsilon''/\epsilon'$)) and boiling point (°C) of the different solvents (Isopropanol ($i\text{PrOH}$), Ethanol (EtOH), Methanol (MeOH))

Solvent	ϵ'	ϵ''	$\tan \delta$	Boiling point
$i\text{PrOH}$	19.9	15.9	0.799	82
EtOH	24.3	22.9	0.941	78
MeOH	32.6	21.5	0.659	65

TEM image

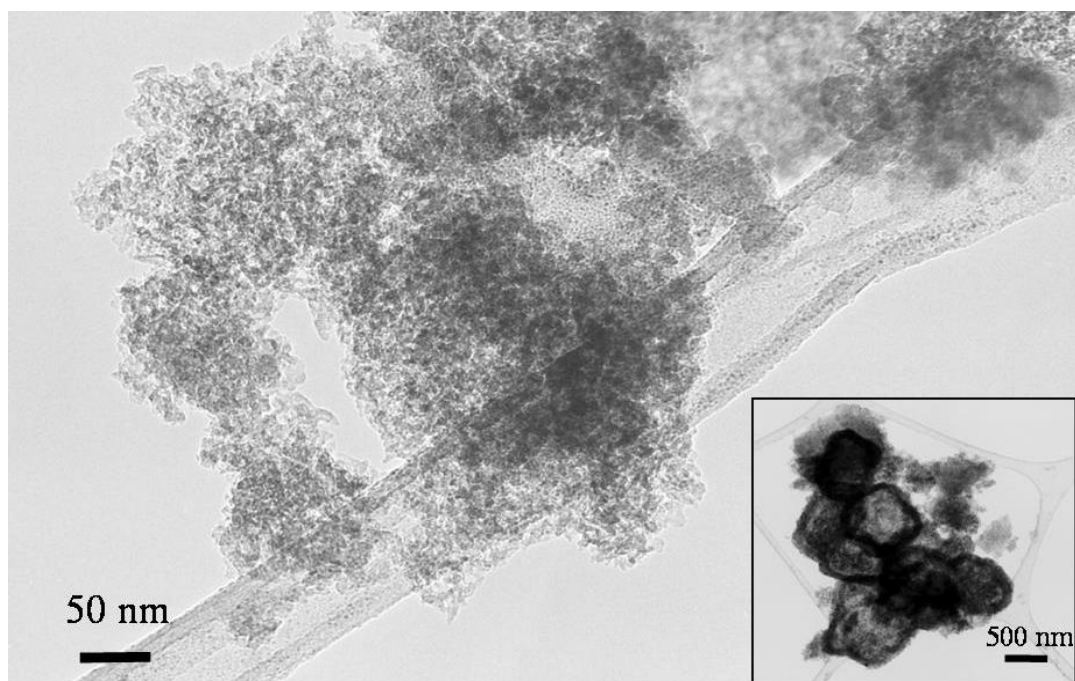


Figure S4. Low resolution TEM image of S-345

Solid State NMR

^{19}F decoupling

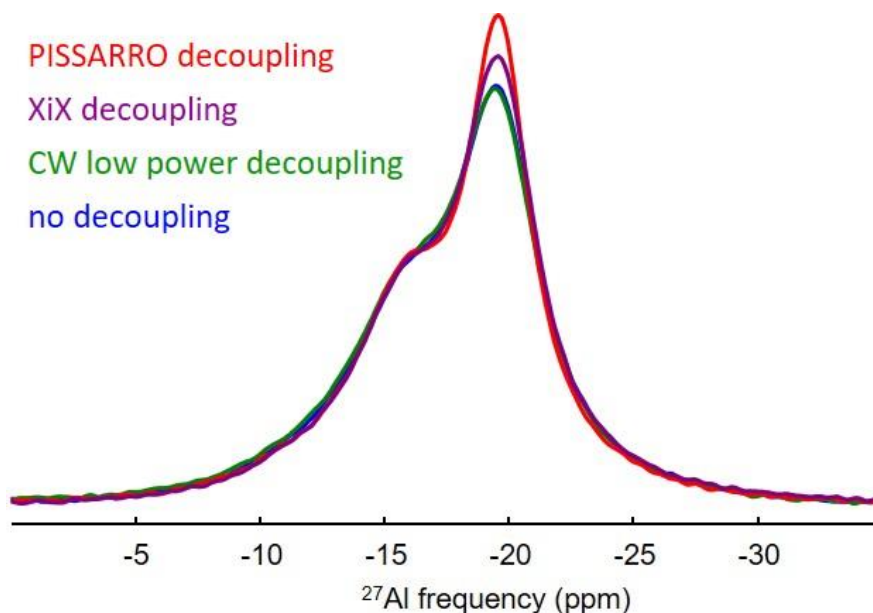


Figure S5. ^{27}Al MAS (33 kHz) NMR spectra of S-185 recorded at 17.6 T without (in blue) and with ^{19}F decoupling using three different decoupling schemes (in green, mauve and red).³⁻⁵ The decoupling sequences have been optimized and the best ^{19}F decoupling efficiency at a MAS frequency of 33 kHz is obtained using the PISSARRO decoupling (in red).⁵

Bibliographic data on ^{27}Al δ_{iso} values of aluminum hydroxyfluorides and aluminum fluoride hydrate

Table S4. ^{27}Al δ_{iso} (ppm) of the ^{27}Al NMR lines assigned to $\text{AlF}_{6-y}(\text{OH})_y$ or $\text{AlF}_{6-y}(\text{OH}_2)_y$ environments of aluminum hydroxyfluorides and aluminum fluoride hydrate.

Compound	y=0	y=1	y=2	y=3	y=4	y=5
$\beta\text{-AlF}_{2.4}(\text{OH})_{0.6}$ ⁶	-15.5	-15.5	-11.7	-7.7		
$\beta\text{-AlF}_{2.6}(\text{OH})_{0.4}$ ⁶	-15.5	-15.5	-11.7	-9.5		
Pyrochlore $\text{AlF}_{1.8}(\text{OH})_{1.2}$ 0.3 H_2O ⁷	-12.5	-12.5	-12.5	-8.7	-4.2	1.8
$\beta\text{-AlF}_{2.6}(\text{OH})_{0.4}$ (annealed 873 K) ⁸	-15.6	-15.6	-11.6			
$\text{Al}_{0.82}\square_{0.18}\text{F}_{2.46}(\text{H}_2\text{O})_{0.54}$ ⁹	-17.9	-14.4	-11.7	-9.4		
Pyrochlore $\text{AlF}_{1.4-1.9}(\text{OH})_{1.6-1.1}$ H_2O ¹⁰	nd ⁽¹⁾	-9.4 to -6.8	-4.5 to -2.6	0.6 to 1.8	2.3 to 4.9	9.7 & 11.4

⁽¹⁾ $\delta^{27}\text{Al} = -15.8$ and -16.7 ppm

^{27}Al isotropic chemical shift ranges and quadrupolar coupling constants of the various $\text{AlF}_{6-y}(\text{OH})_y$ species and ^{19}F isotropic chemical shift ranges of the various $\text{AlF}_2\text{F}_{10-z}(\text{OH})_z$ species calculated using the DFT-GIPAW method for 2x1x1 supercell structural models

All Density Functional Theory (DFT) computations were performed with the Castep code^{11,12} using the PBE functional¹³ and ultrasoft pseudopotential¹⁴ generated “on-the-fly” as described in previous works.^{15,16} A plane wave basis set energy cut-off of 600 eV and a Monkhorst-Pack grid density equal to 0.04 Å⁻¹ were used. The chemical shieldings for ^{19}F and ^{27}Al and the quadrupolar coupling NMR parameters for ^{27}Al were computed using the GIPAW¹⁷ and PAW¹⁸ methods, respectively. ^{27}Al calculated isotropic shieldings were converted to calculated isotropic chemical shifts using calculated and experimental¹⁹ values for $\beta\text{-AlF}_3$ as secondary reference with the relation δ_{iso} (ppm) = - σ_{iso} + 548.2. ^{19}F calculated isotropic shieldings were converted to calculated isotropic chemical shifts using the relationship previously established with the same computational parameters.^{15,20}

Models consisting of 2x1x1 supercells of the $\beta\text{-AlF}_3$ unit cell with chemical compositions $\text{AlF}_2(\text{OH})$ and $\text{AlF}_{1.875}(\text{OH})_{1.125}$ were considered (cell parameters (Å): $a = 13.862$, $b = 12.002$ and $c = 7.134$). 16 structures with random distributions of OH groups on the F1 and F2 sites ($\text{AlF}_2(\text{OH})$) and 8 structures with random distributions of OH groups on all F sites ($\text{AlF}_{1.875}(\text{OH})_{1.125}$) were randomly generated using the supercell code.²¹ Atomic positions of these 24 structures were optimized by DFT keeping cell parameters fixed. The cif files of the 24 supercell structural models are available as SI.

Table S5. Average calculated ^{27}Al isotropic chemical shift (δ_{iso} , ppm) of the $\text{AlF}_{6-y}(\text{OH})_y$ species found in the (a) 16 $\text{AlF}_2(\text{OH})$ and (b) 8 $\text{AlF}_{1.875}(\text{OH})_{1.125}$ supercell models accounting for distributions of OH group in (a) only F1 and F2 sites and (b) all F sites of the structure.

y	Amount of species (a)	δ_{iso}	Amount of species (b)	δ_{iso}
0	7	-11.9	2	-10.6
1	70	-6.1	29	-6.0
2	227	-0.8	84	-1.0
3	76	3.3	73	2.9
4	4	6.8	4	6.7

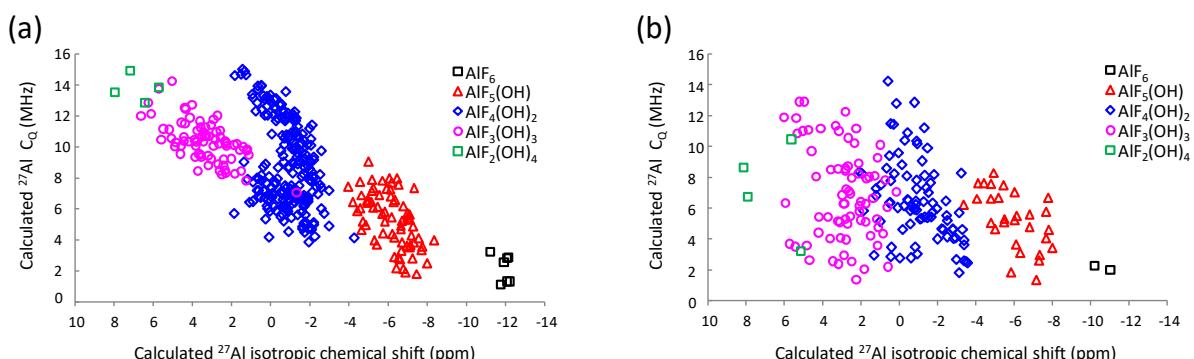


Figure S6. Calculated ^{27}Al quadrupolar coupling constants (C_Q) as a function of the calculated ^{27}Al isotropic chemical shifts of the various $\text{AlF}_{6-y}(\text{OH})_y$ species found in the (a) 16 $\text{AlF}_2(\text{OH})$ and (b) 8 $\text{AlF}_{1.875}(\text{OH})_{1.125}$ supercell models, considering a distribution of OH group in (a) only F1 and F2 sites and (b) all F sites of the structure.

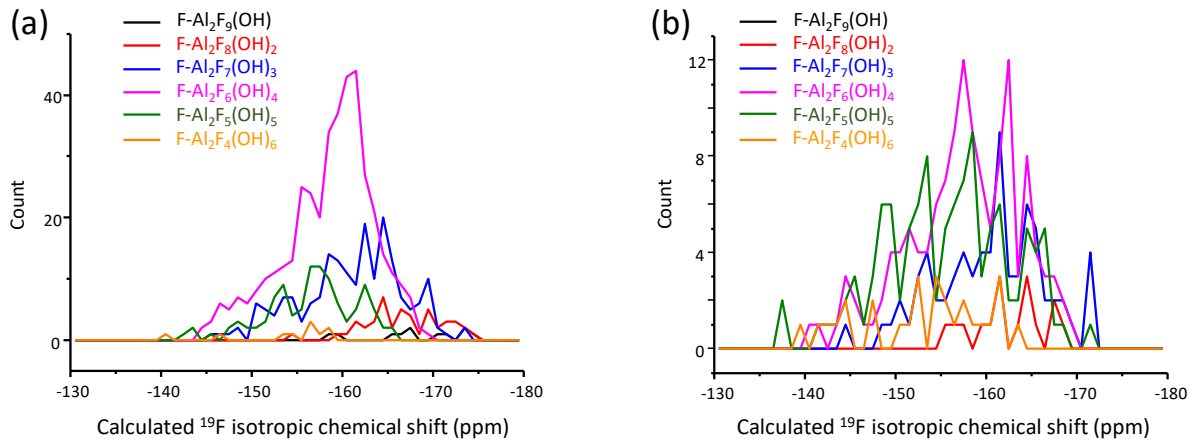


Figure S7. Histogram of the calculated ^{19}F isotropic chemical shifts of the various $\text{FAl}_2\text{F}_{10-z}(\text{OH})_z$ species found in the (a) 16 $\text{AlF}_2(\text{OH})$ and (b) 8 $\text{AlF}_{1.875}(\text{OH})_{1.125}$ supercell models, with chemical composition $\text{AlF}_2(\text{OH})$, considering a distribution of OH group in (a) only F1 and F2 sites and (b) all F sites of the structure.

Table S6. Average calculated ^{19}F isotropic chemical shift (δ_{iso} , ppm) of the various $\text{FAl}_2\text{F}_{10-z}(\text{OH})_z$ species found in the (a) 16 $\text{AlF}_2(\text{OH})$ and (b) 8 $\text{AlF}_{1.875}(\text{OH})_{1.125}$ supercell models, accounting for distributions of OH group in (a) only F1 and F2 sites and (b) all F sites of the structure.

z	Amount of species (a)	δ_{iso} (a)	Amount of species (b)	δ_{iso} (b)
1	11	-167.9	0	
2	46	-166.7	16	-162.6
3	192	-161.0	72	-160.4
4	402	-158.6	132	-157.6
5	107	-156.6	111	-155.7
6	10	-153.9	28	-153.0
7	0		1	-153.5

^{27}Al MAS (33 kHz) NMR spectra of $\beta\text{-AlF}_{3-x}(\text{OH})_x$ samples

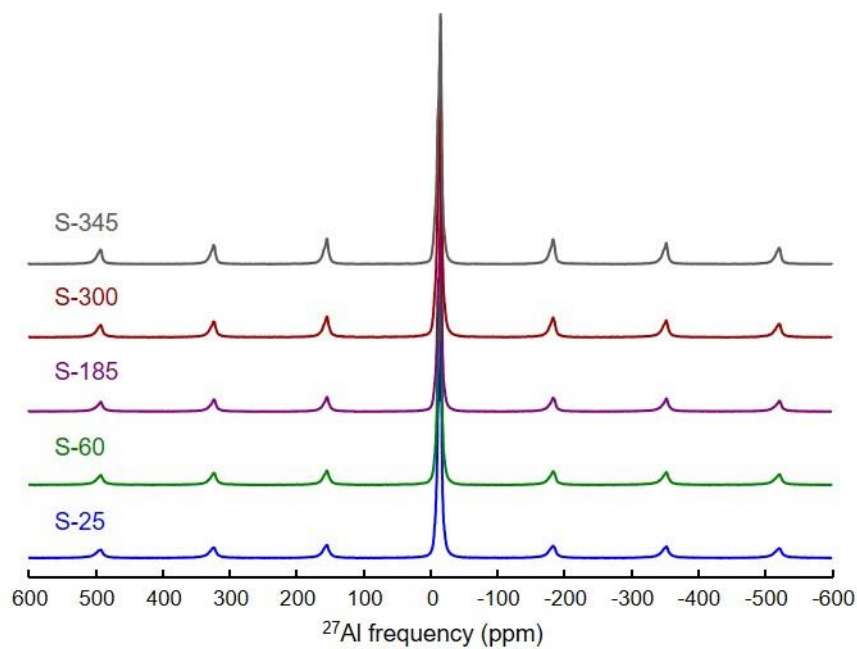


Figure S8. ^{27}Al MAS (33 kHz) NMR spectra of $\beta\text{-AlF}_{3-x}(\text{OH})_x$ samples recorded at 17.6 T.

Structural data of β -AlF₃

Table S7. Al-F (AlF₆ octahedra), F-Al and F-F (FAI₂F₈ environments) distances (d, Å) in β -AlF₃.²²

Atom 1	Atom 2	d	Atom 1	Atom 2	d
Al1	F3 (x2)	1.7961	Al2	F4 (x2)	1.7978
	F2 (x4)	1.8015		F1 (x2)	1.7996
F1	Al2 (x2)	1.7996	F3	Al1 (x2)	1.7961
	F2 (x2)	2.5405		F2 (x4)	2.5383
	F4 (x2)	2.5425		F2 (x4)	2.5495
	F4 (x2)	2.5451	F4	Al2 (x2)	1.7978
	F2 (x2)	2.5510		F2 (x2)	2.5403
F2	Al2	1.8006		F1 (x2)	2.5425
	Al1	1.8015		F1 (x2)	2.5451
	F3	2.5383		F2 (x2)	2.5487
	F4	2.5403			
	F1	2.5405			
	F2	2.5461			
	F4	2.5487			
	F2	2.5492			
	F3	2.5495			
	F1	2.5510			

^{19}F MAS experimental and reconstructed spectra of $\beta\text{-AlF}_{3-x}(\text{OH})_x$ samples

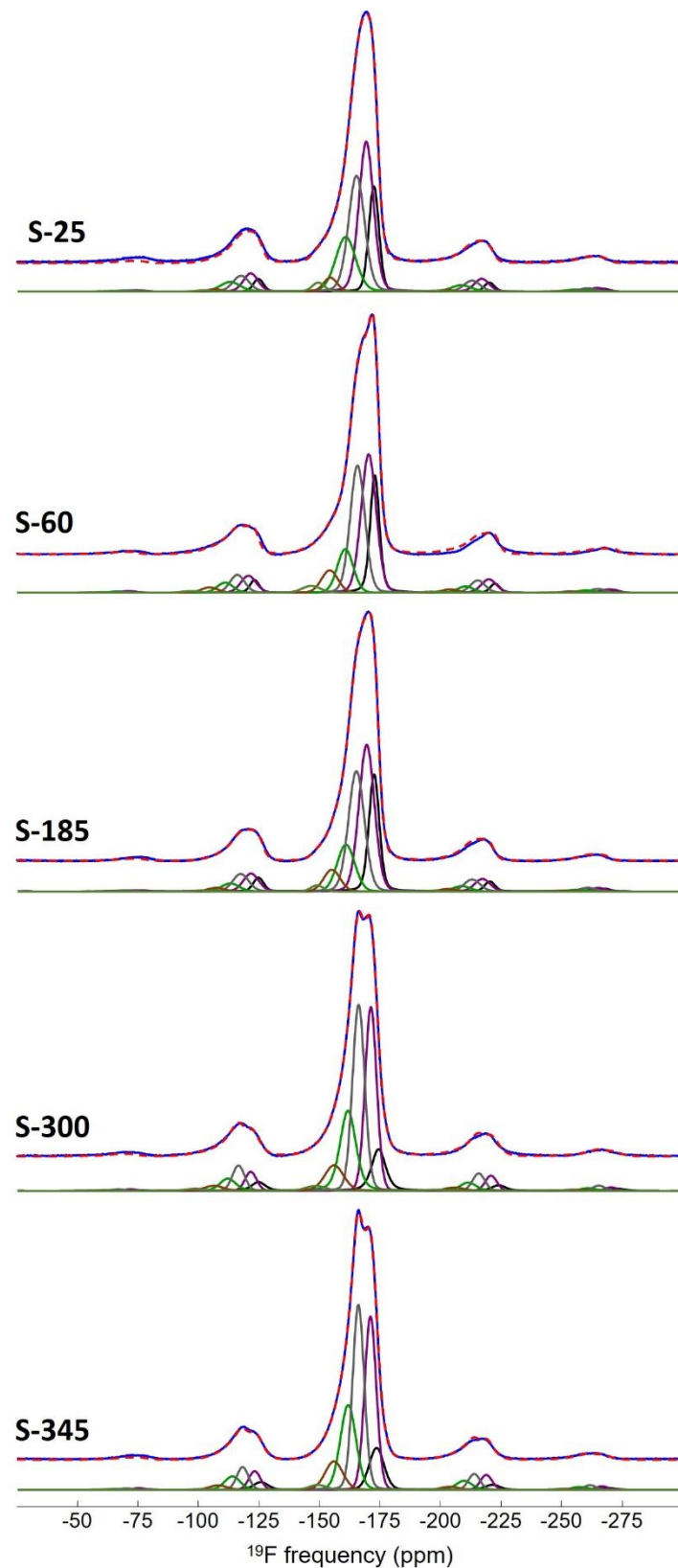


Figure S9. ^{19}F MAS (33 kHz) experimental (in blue) spectra recorded at 17.6 T of $\beta\text{-AlF}_{3-x}(\text{OH})_x$ samples with SSA of 25, 60, 185, 300 and 345 m^2/g and their reconstructions (dashed red lines). For each spectrum, the six individual resonances used for the fit are shown below.

References

- (1) Box, G. E. P.; Hunter, J. S.; Hunter, W. G. *Statistics for Experimenters: Design, Innovation, and Discovery*, 2nd ed.; Wiley series in probability and statistics; Wiley-Interscience: Hoboken, N.J, 2005.
- (2) Plackett, R. L.; Burman, J. P. THE DESIGN OF OPTIMUM MULTIFACTORIAL EXPERIMENTS. *Biometrika* **1946**, 33 (4), 305–325. <https://doi.org/10.1093/biomet/33.4.305>.
- (3) Ernst, M.; Samoson, A.; Meier, B. H. Low-Power Decoupling in Fast Magic-Angle Spinning NMR. *Chemical Physics Letters* **2001**, 348 (3–4), 293–302. [https://doi.org/10.1016/S0009-2614\(01\)01115-0](https://doi.org/10.1016/S0009-2614(01)01115-0).
- (4) Detken, A.; Hardy, E. H.; Ernst, M.; Meier, B. H. Simple and Efficient Decoupling in Magic-Angle Spinning Solid-State NMR: The XiX Scheme. *Chemical Physics Letters* **2002**, 356 (3–4), 298–304. [https://doi.org/10.1016/S0009-2614\(02\)00335-4](https://doi.org/10.1016/S0009-2614(02)00335-4).
- (5) Weingarth, M.; Tekely, P.; Bodenhausen, G. Efficient Heteronuclear Decoupling by Quenching Rotary Resonance in Solid-State NMR. *Chemical Physics Letters* **2008**, 466 (4–6), 247–251. <https://doi.org/10.1016/j.cplett.2008.10.041>.
- (6) Dambournet, D.; Demourgues, A.; Martineau, C.; Pechev, S.; Lhoste, J.; Majimel, J.; Vimont, A.; Lavalle, J.-C.; Legein, C.; Buzaré, J.-Y.; Fayon, F.; Tressaud, A. Nanostructured Aluminium Hydroxyfluorides Derived from β -AlF₃. *Chem. Mater.* **2008**, 20 (4), 1459–1469. <https://doi.org/10.1021/cm702603b>.
- (7) Dambournet, D.; Demourgues, A.; Martineau, C.; Durand, E.; Majimel, J.; Vimont, A.; Leclerc, H.; Lavalle, J.-C.; Daturi, M.; Legein, C.; Buzaré, J.-Y.; Fayon, F.; Tressaud, A. Structural Investigations and Acidic Properties of High Surface Area Pyrochlore Aluminium Hydroxyfluoride. *J. Mater. Chem.* **2008**, 18 (21), 2483. <https://doi.org/10.1039/b718856k>.
- (8) Dambournet, D.; Demourgues, A.; Martineau, C.; Majimel, J.; Feist, M.; Legein, C.; Buzaré, J.-Y.; Fayon, F.; Tressaud, A. Nanostructured Al-Based Fluoride-Oxide Materials with a Core-Shell Morphology. *J. Phys. Chem. C* **2008**, 112 (32), 12374–12380. <https://doi.org/10.1021/jp801310e>.
- (9) Dambournet, D.; Demourgues, A.; Martineau, C.; Durand, E.; Majimel, J.; Legein, C.; Buzaré, J.-Y.; Fayon, F.; Vimont, A.; Leclerc, H.; Tressaud, A. Microwave Synthesis of an Aluminum Fluoride Hydrate with Cationic Vacancies: Structure, Thermal Stability, and Acidic Properties. *Chem. Mater.* **2008**, 20 (22), 7095–7106. <https://doi.org/10.1021/cm8023617>.
- (10) König, R.; Scholz, G.; Pawlik, A.; Jäger, C.; van Rossum, B.; Oschkinat, H.; Kemnitz, E. Crystalline Aluminum Hydroxy Fluorides: Structural Insights Obtained by High Field Solid State NMR and Trend Analyses. *J. Phys. Chem. C* **2008**, 112 (40), 15708–15720. <https://doi.org/10.1021/jp804662f>.
- (11) Segall, M. D.; Lindan, P. J. D.; Probert, M. J.; Pickard, C. J.; Hasnip, P. J.; Clark, S. J.; Payne, M. C. First-Principles Simulation: Ideas, Illustrations and the CASTEP Code. *J. Phys.: Condens. Matter* **2002**, 14 (11), 2717–2744. <https://doi.org/10.1088/0953-8984/14/11/301>.

- (12) Clark, S. J.; Segall, M. D.; Pickard, C. J.; Hasnip, P. J.; Probert, M. I. J.; Refson, K.; Payne, M. C. First Principles Methods Using CASTEP. *Zeitschrift für Kristallographie - Crystalline Materials* **2005**, 220 (5/6). <https://doi.org/10.1524/zkri.220.5.567.65075>.
- (13) Perdew, J. P.; Burke, K.; Ernzerhof, M. Generalized Gradient Approximation Made Simple. *Physical Review Letters* **1996**, 77 (18), 3865–3868. <https://doi.org/10.1103/PhysRevLett.77.3865>.
- (14) Yates, J. R.; Pickard, C. J.; Mauri, F. Calculation of NMR Chemical Shifts for Extended Systems Using Ultrasoft Pseudopotentials. *Physical Review B* **2007**, 76 (2). <https://doi.org/10.1103/PhysRevB.76.024401>.
- (15) Sadoc, A.; Body, M.; Legein, C.; Biswal, M.; Fayon, F.; Rocquefelte, X.; Boucher, F. NMR Parameters in Alkali, Alkaline Earth and Rare Earth Fluorides from First Principle Calculations. *Physical Chemistry Chemical Physics* **2011**, 13 (41), 18539. <https://doi.org/10.1039/c1cp21253b>.
- (16) Cadars, S.; Guégan, R.; Garaga, M. N.; Bourrat, X.; Le Forestier, L.; Fayon, F.; Huynh, T. V.; Allier, T.; Nour, Z.; Massiot, D. New Insights into the Molecular Structures, Compositions, and Cation Distributions in Synthetic and Natural Montmorillonite Clays. *Chem. Mater.* **2012**, 24 (22), 4376–4389. <https://doi.org/10.1021/cm302549k>.
- (17) Pickard, C. J.; Mauri, F. All-Electron Magnetic Response with Pseudopotentials: NMR Chemical Shifts. *Physical Review B* **2001**, 63 (24). <https://doi.org/10.1103/PhysRevB.63.245101>.
- (18) Profeta, M.; Mauri, F.; Pickard, C. J. Accurate First Principles Prediction of ^{17}O NMR Parameters in SiO_2 : Assignment of the Zeolite Ferrierite Spectrum. *J. Am. Chem. Soc.* **2003**, 125 (2), 541–548. <https://doi.org/10.1021/ja027124r>.
- (19) Chupas, P. J.; Ciraolo, M. F.; Hanson, J. C.; Grey, C. P. In Situ X-Ray Diffraction and Solid-State NMR Study of the Fluorination of $\gamma\text{-Al}_2\text{O}_3$ with HCF_2Cl . *Journal of the American Chemical Society* **2001**, 123 (8), 1694–1702. <https://doi.org/10.1021/ja0032374>.
- (20) Sadoc, A.; Biswal, M.; Body, M.; Legein, C.; Boucher, F.; Massiot, D.; Fayon, F. NMR Parameters in Column 13 Metal Fluoride Compounds (AlF_3 , GaF_3 , InF_3 and TlF) from First Principle Calculations. *Solid State Nuclear Magnetic Resonance* **2014**, 59–60, 1–7. <https://doi.org/10.1016/j.ssnmr.2014.01.001>.
- (21) Okhotnikov, K.; Charpentier, T.; Cadars, S. Supercell Program: A Combinatorial Structure-Generation Approach for the Local-Level Modeling of Atomic Substitutions and Partial Occupancies in Crystals. *J. Cheminform* **2016**, 8 (1), 17. <https://doi.org/10.1186/s13321-016-0129-3>.
- (22) Le Bail, A.; Jacoboni, C.; Leblanc, M.; De Pape, R.; Duroy, H.; Fourquet, J. L. Crystal Structure of the Metastable Form of Aluminum Trifluoride $\beta\text{-AlF}_3$ and the Gallium and Indium Homologs. *Journal of Solid State Chemistry* **1988**, 77 (1), 96–101. [https://doi.org/10.1016/0022-4596\(88\)90095-3](https://doi.org/10.1016/0022-4596(88)90095-3).